Solely biobased strain sensor with ultra-precision response via surface graphitization strategy

Zhihao Yang, Ying Yuan, Bin Wang, Xiaojun Shen, Xiluan Wang* and Tong-Qi Yuan*

Beijing Key Laboratory of Lignocellulosic Chemistry, Beijing Forestry University, Beijing 100083, China.

*Corresponding author: Beijing Key Laboratory of Lignocellulosic Chemistry, Beijing Forestry University. E-mails: wangxiluan@bjfu.edu.cn; ytq581234@bjfu.edu.cn

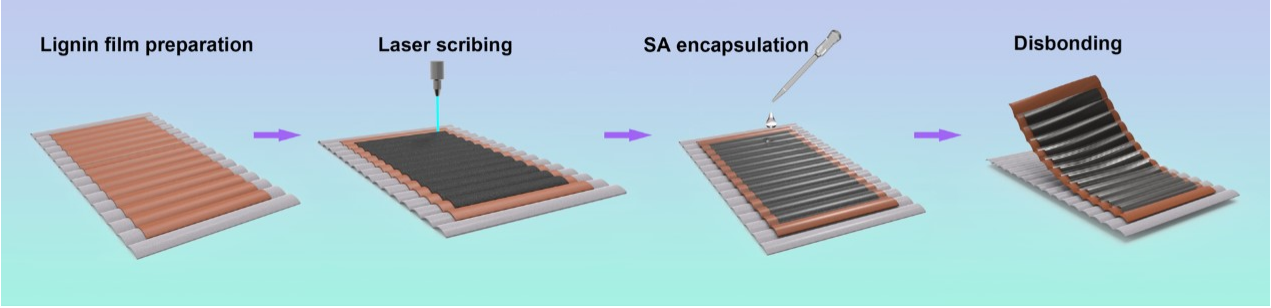

Fig. S1 Detailed preparation process of SBBS.

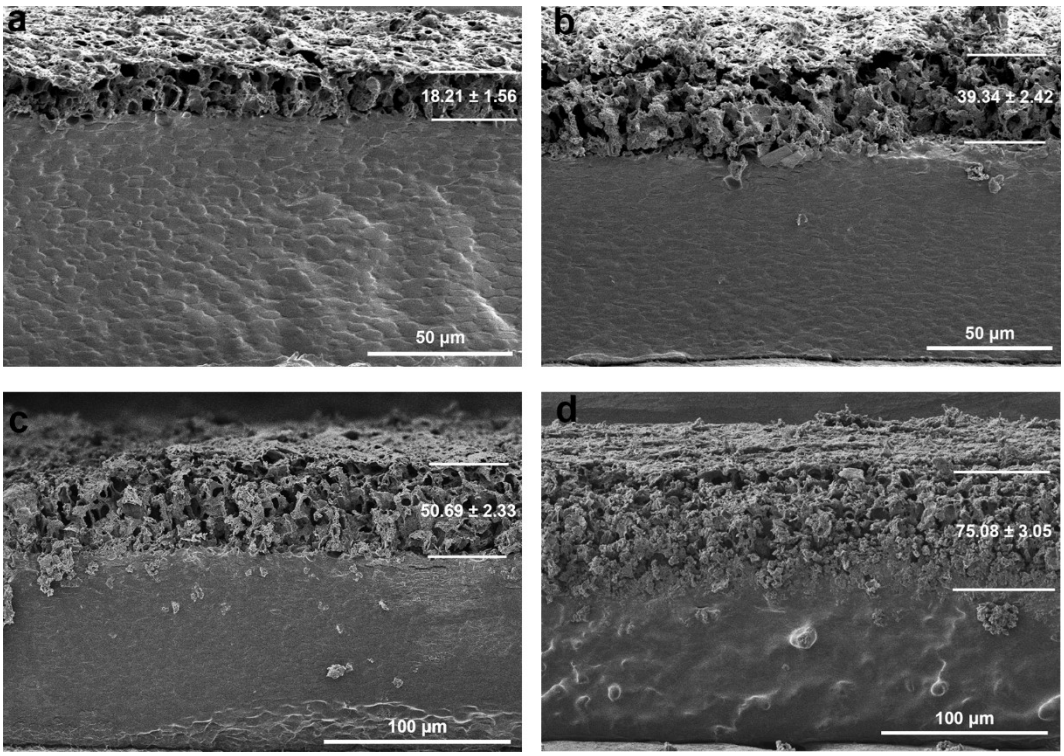

Fig. S2 The cross section of LIG was obtained by different laser power. a) LIG-P35. b) LIG-P40. c) LIG-P45. d) LIG-P50.

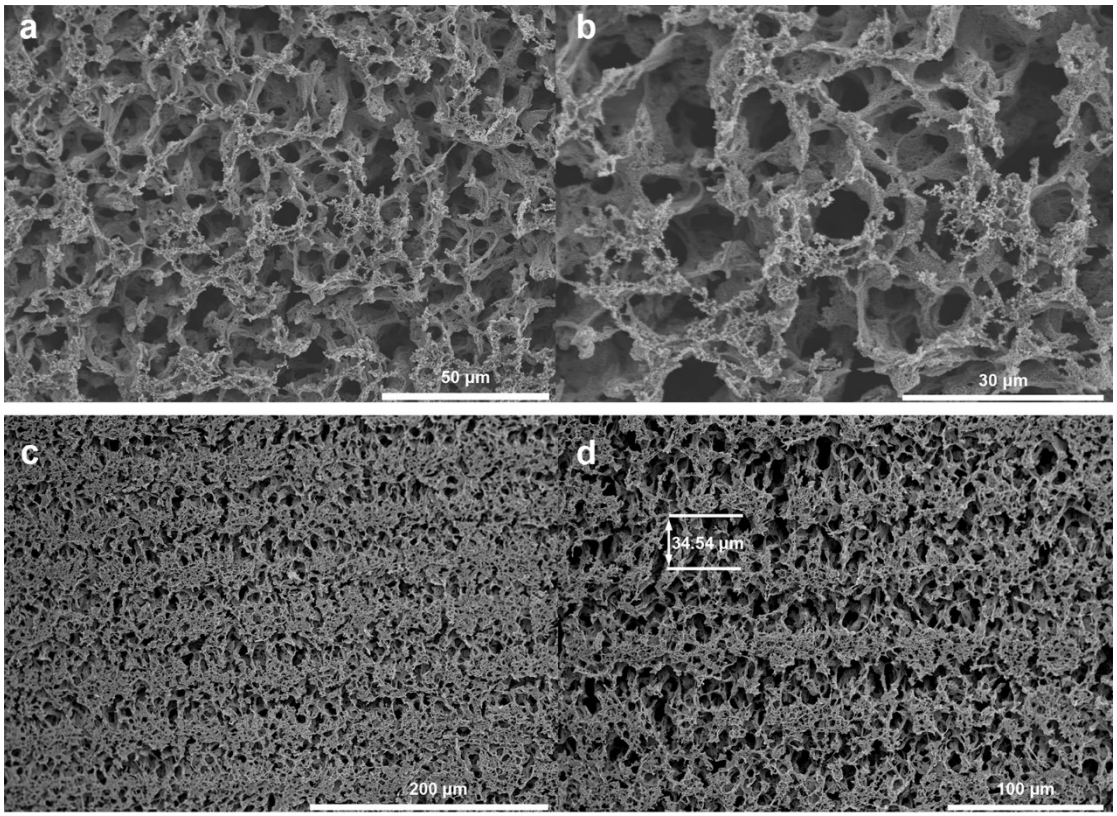

Fig. S3 Surface SEM images of LIG. a, b) Surface uniform porous structure. c, d) Streaks produced by laser reduction.

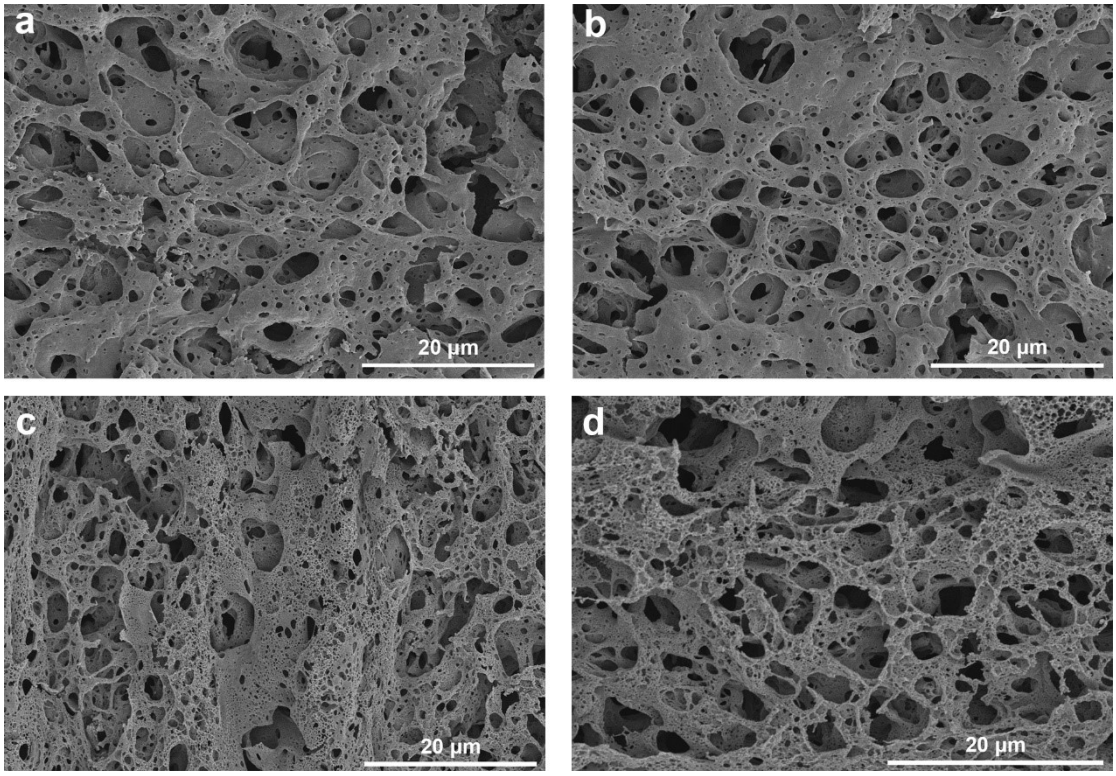

Fig. S4 LIG porous structures prepared by different laser power. a), b), c), d) are the LIG prepared under the laser power of 35%,40%,45%,50%, respectively.

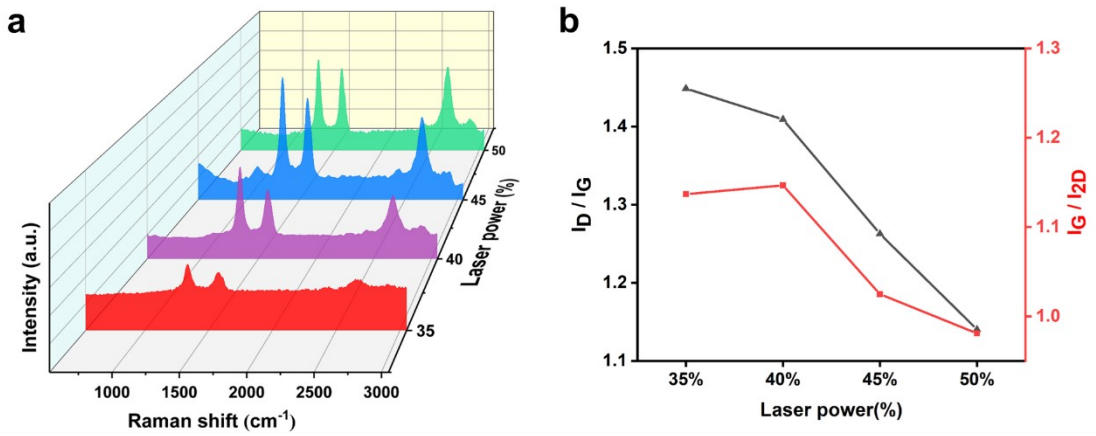

Fig. S5 Raman characterization of LIG under different laser power reductions (AL:SA = 4:1). a) Raman spectra of LIG under different laser power reductions. b) Calculate the ratio of D peak to G peak, and the ratio of G peak to 2D peak in Raman spectrum of LIG obtained by different laser power reduction.

Figure S2a shows that LIG has high G and 2D peaks. LIG-P35 represents the LIG generated at 35% etching power, and so on. When the power is 35%, there is an obvious D peak and G peak, but no obvious 2D peak. When the laser power is increased from 35 to 50%, the intensity of peak D increases somewhat, but the intensity of peaks G and 2D increases significantly. The 2D peak shows an increase in its intensity when laser power increased, indicating that structures with fewer layers were being formed, which indicates the formation of high-quality graphite structures. Figure S2b shows the I_D/I_G and I_G/I_{2D} ratio, the I_{2D}/I_G ratio gives a measure on the layered nature of produced graphitic structures. The result showed that the I_D/I_G and I_G/I_{2D} ratio decreased with the change in laser power from 35 to 50%. The lowest I_D/I_G and I_G/I_{2D} ratios were 1.14 and 0.98, respectively, at 50% power etching.

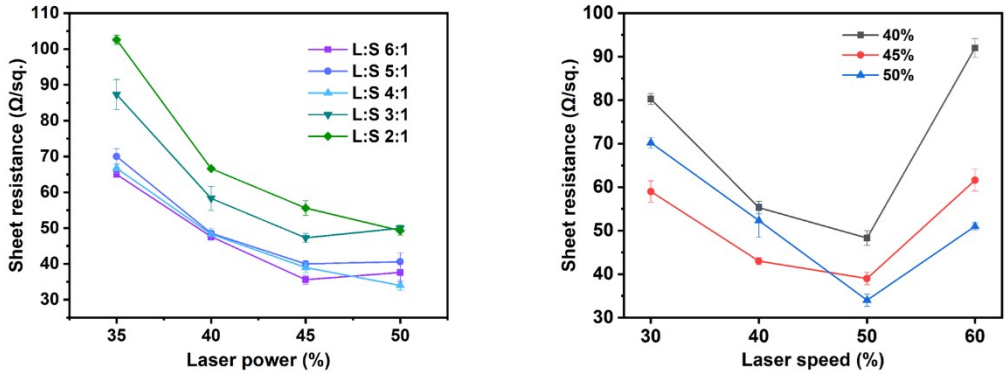

Fig. S6 LIG sheet resistance obtained by different processes. a) The sheet resistance of LIG under different AL:SA and different laser power. b) The sheet resistance of LIG was obtained at different laser etching speed and different laser power.

The optimal preparation parameters of LIG are determined by controlling variables, as shown in Figures S2a and S2b. Figure S2a shows the effect of different AL:SA ratios and laser power on the sheet resistance of LIG. It can be intuitively seen that as the laser power increases gradually, the sheet resistance decreases gradually. However, when the laser power exceeds 50%, the LIG appears broken. In the AL:SA system, as the proportion of AL increases, the sheet resistance decreases first and then increases. When AL:SA is 4:1, the sheet resistance decreases to 34 Ω sq^{-1}. Figure S2b shows the effect of laser speed and laser power on the sheet resistance of LIG. When the laser power increases from 35 to 50%, the sheet resistance trend of change is "U" shaped. When the laser power is 50% and the laser speed is 50%, the lowest value of sheet resistance is obtained. In conclusion, AL:SA ratio is 4:1, laser power and laser speed are 50% are the best preparation parameters of LIG.

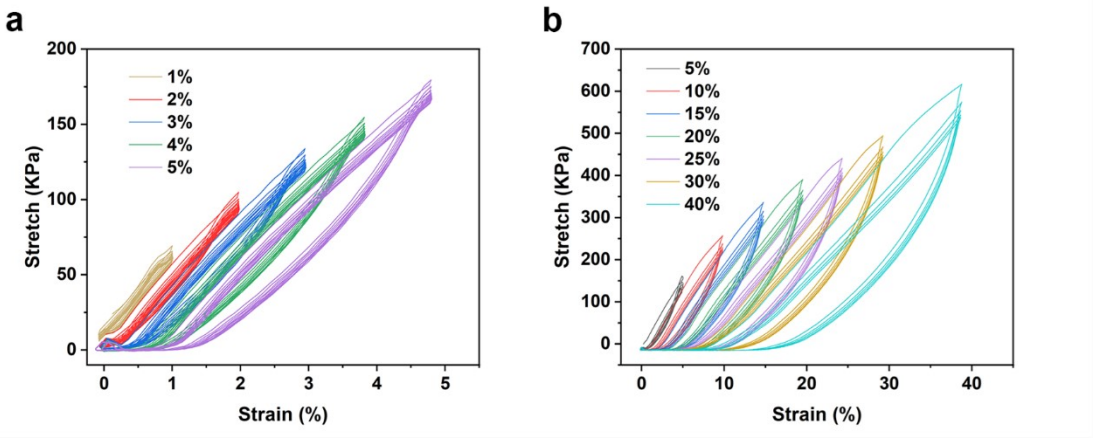

Fig. S7 Mechanical property characterization. a) Stretch from 1 to 5% with 10 stretching cycles per set. b) Stretch from 5 to 40% with 5 stretching cycles per set.

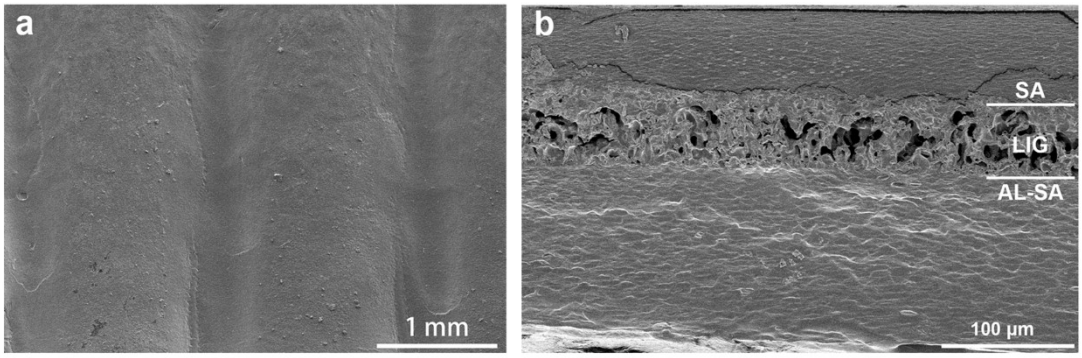

Fig. S8 The SEM of the SBBS after 5000 cycles mechanical tests. a) Surface of SBBS. b) Cross-section of SBBS.

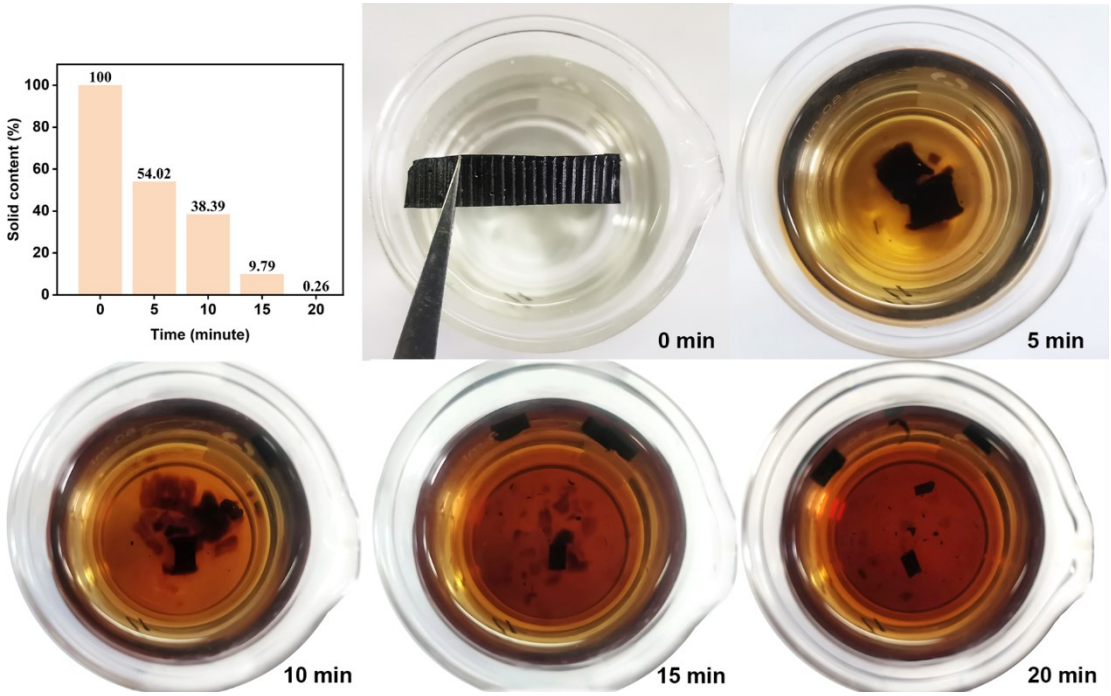

Fig. S9 Sensor water solubility demonstration. Water temperature is 70 ℃.

Table S1 Comparison of sensing performance in the same field.

Sensor materials		GF		Max strain (%)	Linear(R^2)	Stability	References
XSBR/SSCNT	4.24	25.98		220	-	-	S1
Ag/PDMS	940.5	2742.3		22.5	-	8000	22
CNT/PDMS	2.5	3.4		130	-	10000	18
MXene/CNT	64.6	772.6		70	-	5000	S2
Graphene/Ecoflex	0.6	17.4		200	-	-	54
CB/PANIP/TPU	197.2	1080	3030.8	700	-	10000	S3
Graphene/PVDF/TPU	51	87		8	0.98; 0.99	6000	S4
CCF/Ecoflex	25	65		140	-	2000	S5
TPU/MWCNTs/MXene	13	73	363	80	0.90; 0.95	2000	S6
CNT/TPU	0.101	0.0333		600	0.996; 0.980	2000	S7
CNT/TPU	16.47	99.73; 373.96	1189.19	221	0.969; 0.977 0.989; 0.967	5000	19
LIG/Ecoflex		4.51	43.92	50	0.98; 0.99	7250	S8
LIG/PEEK/PDMS	18.3	207.5	1814	14	-	15000	S9
LIG/GO/PDMS	96	218	1242.3	50	-	2500	21
LIG/GO/PDMS	33.4	85.1	387.4	7.5	-	-	S10
LIG/PI/Starch	20.5	134.2		0.8	-	1000	S11
rGO/PDMS/VHB	19.24 ; 170.7	9156.29; 55785.76	167665.61	300	0.98; 0.81; 0.949;0.98; 0.996	10000	S12
GO/CNT/PVA/AM/AA		20		300	0.99	5000	S13
This work		46.65		80	0.99903	5000	

References

S1 M. Lin, Z. Zheng, L. Yang, M. Luo, L. Fu, B. Lin and C. Xu, *Adv. Mater.*, 2022, **34**, e2107309.

S2 Y. Cai, J. Shen, G. Ge, Y. Zhang, W. Jin, W. Huang, J. Shao, J. Yang and X. Dong, *ACS Nano*, 2017, **12**, 56-62.

S3 W. Zhai, J. Zhu, Z. Wang, Y. Zhao, P. Zhan, S. Wang, G. Zheng, C. Shao, K. Dai, C. Liu and C. Shen, *ACS Appl. Mater. Interfaces*, 2022, **14**, 4562-4570.

S4 T. Huang, P. He, R. Wang, S. Yang, J. Sun, X. Xie and G. Ding, *Adv. Funct. Mater.*, 2019, **29,** 1903732.

S5 M. Zhang, C. Wang, H. Wang, M. Jian, X. Hao and Y. Zhang, *Adv. Funct. Mater.*, 2017, **27**, 1604795.

S6 H. Wang, R. Zhou, D. Li, L. Zhang, G. Ren, L. Wang, J. Liu, D. Wang, Z. Tang, G. Lu, G. Sun, H. D. Yu and W. Huang, *ACS Nano*, 2021, **15**, 9690-9700.

S7 H. Li, J. Chen, X. Chang, Y. Xu, G. Zhao, Y. Zhu and Y. Li, *J. Mater. Chem. A*, 2021, **9**, 1795-1802.

S8 W. Wang, L. Lu, Z. Li, L. Lin, Z. Liang, X. Lu and Y. Xie, *ACS Appl. Mater. Interfaces*, 2022, **14**, 1315-1325.

S9 Q. Li, T. Wu, W. Zhao, J. Ji and G. Wang, *ACS Appl. Mater. Interfaces*, 2021, **13**, 37433-37444.

S10 D. Y. Wang, L. Q. Tao, Y. Liu, T. Y. Zhang, Y. Pang, Q. Wang, S. Jiang, Y. Yang and T. L. Ren, *Nanoscale*, 2016, **8**, 20090-20095.

S11 W. Yang, W. Zhao, Q. Li, H. Li, Y. Wang, Y. Li and G. Wang, *ACS Appl. Mater. Interfaces*, 2020, **12**, 3928-3935.

S12 Z. Chu, W. Jiao, Y. Huang, Y. Zheng, R. Wang and X. He, *J. Mater. Chem. A*, 2021, **9**, 9634-9643.

S13 A. Chen, J. Zhang, J. Zhu, Z. Yan, Q. Wu, S. Han, J. Huang and L. Guan, *J. Mater. Chem. A*, 2023, **11**, 4977-4986.